

## Nuclear Halo and Its Related Reactions

Zhang Huanqiao\*

China Institute of Atomic Energy, 102413 Beijing, China

Received: November 8, 2005

The experimental results of the proton halo nuclei  $^{27}\text{P}$ , as well as probably  $^{29}\text{S}$ , and the neutron halo in excited states of the nuclei  $^{12}\text{B}$  and  $^{13}\text{C}$  are presented. The probability of the valence nucleon(s) being out of the binding potential have been extracted systematically from the relevant experimental data, and a new condition for nuclear halo occurrence is proposed. Based on our systematical study, we put forward our scaling laws of nuclear halo in terms of the analytical expressions of the expectation value for the operator  $\mathbf{r}^2$  in a finite square-well potential. In order to investigate the breakup effects of the weakly bound projectiles on fusion reactions and barrier distributions, the complete fusion cross sections of  $^6\text{Li} + ^{208}\text{Pb}$  and the elastic and quasi-elastic excitation functions of  $^6,7\text{Li} + ^9\text{Be} + ^{208}\text{Pb}$  were measured and compared with the predictions of the coupled-channels model. The dynamical effects on fusion of neutron-rich nuclei at the energies around the Coulomb barrier are discussed in terms of the comparison of the measured fusion data of  $^{48}\text{Ca} + ^{90,96}\text{Zr}$  with the calculations of the improved quantum molecular dynamics model and coupled-channels theory.

### 1. Introduction

The neutron and proton density distributions in nucleus are very important quantities for understanding various nuclear properties such as nuclear potential, single-particle orbits, and magic numbers. So far, the experimental and theoretical studies of the nuclear density distributions have resulted in a lot of basic and meaningful information on nuclear structures. One of the most notable results is the discovery of two-neutron halo nucleus  $^{11}\text{Li}$  by Tanihata et al.<sup>1</sup> at Lawrence Berkeley Laboratory in 1985. Nuclear halo is a threshold phenomenon. As the binding energy becomes small, the wave function of valence particle extends more and more outward if the centrifugal barrier is small. Eventually, this leads to the wave function penetrating substantially beyond the range of nuclear force as the binding energy approaches zero, i.e. occurrence of nuclear halo. Nucleus  $^{11}\text{Li}$  can be viewed as a core plus two valence-neutrons. The density distributions of these two neutrons spread out to distances far from the binding potential. Its root mean square (rms) radius can be comparable with the size of  $^{208}\text{Pb}$  nucleus.

In this paper, we will present our main experimental results of the proton halo nuclei  $^{27}\text{P}$ , as well as  $^{29}\text{S}$ , and the neutron halo in excited states of the nuclei  $^{12}\text{B}$  and  $^{13}\text{C}$ . We also systematically have extracted the probability of the valence nucleon(s) being out of the binding potential from the relevant experimental data and proposed a much relaxed condition for nuclear halo occurrence. Based on our systematical study, we put forward our scaling laws of nuclear halo in terms of the analytical expressions of the expectation value for the operator  $\mathbf{r}^2$  in a finite square-well potential. One of the characters of halo nuclei is weak bounding of the valence nucleon(s). Nuclear reactions induced by halo and weakly bound nuclei are a topic of current interest. In order to investigate the breakup effects of the weakly bound projectiles on fusion reactions and barrier distributions, the complete fusion cross sections of  $^6\text{Li} + ^{208}\text{Pb}$  and the elastic and quasi-elastic excitation functions of  $^6,7\text{Li} + ^{208}\text{Pb}$  were measured and compared with the predictions of the coupled-channels model. Finally, we will discuss the dynamical effects on fusion of neutron-rich nuclei at the ener-

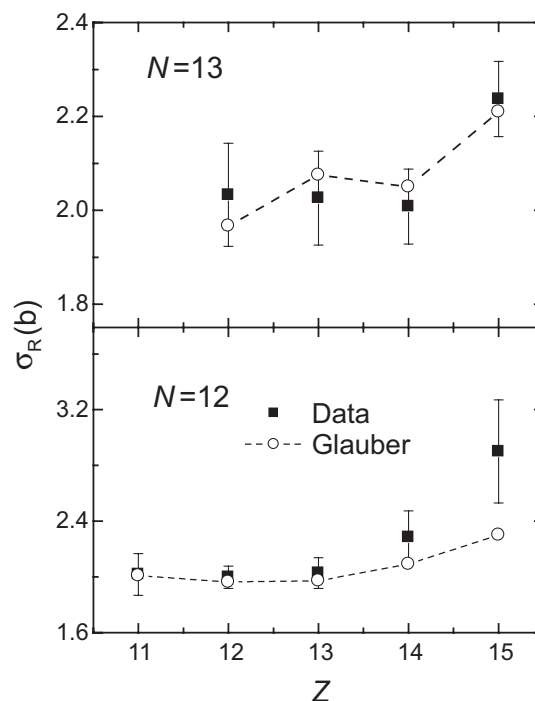


**Figure 1.** The  $Z$  dependence of the reaction cross sections for the isotones with  $N=12$  and  $N=13$ . The solid squares with error bar represent the experimental data. The open circles illustrate the prediction of the modified Glauber model in the OL approach. The symbols are connected by lines for each isotonic number to guide the eye.

gies around the Coulomb barrier in terms of the comparison of the measured fusion data of  $^{48}\text{Ca} + ^{90,96}\text{Zr}$ <sup>2,3</sup> with the calculations of the improved quantum molecular dynamics (ImQMD) model.<sup>4</sup>

### 2. Proton Halo

The existence of proton halos in  $^{26}\text{P}$  and  $^{27}\text{S}$  was first predicted by Ren et al.<sup>5</sup> By further investigation, Brown and Hansen<sup>6</sup> pointed out that  $^{26,27}\text{P}$  and  $^{27,29}\text{S}$  are good candidates for halo nuclei. The properties of proton-rich nuclei in the 2s1d shell were also investigated in the framework of relativistic mean-field model by Chen et al.<sup>7</sup> Their results show that there

\*Corresponding author. E-mail: huan@iris.ciae.ac.cn. Fax: 0086-10-69357787

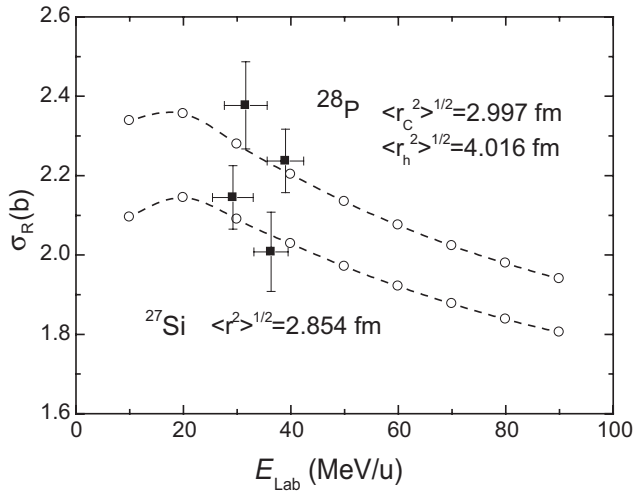


**Figure 2.** The measured reaction cross sections vs energy for the  $^{27}\text{Si}$ ,  $^{28}\text{P}+^{28}\text{Si}$  reactions. The predictions of the modified Glauber model of the OL approach (open circles) are compared with the experimental data.

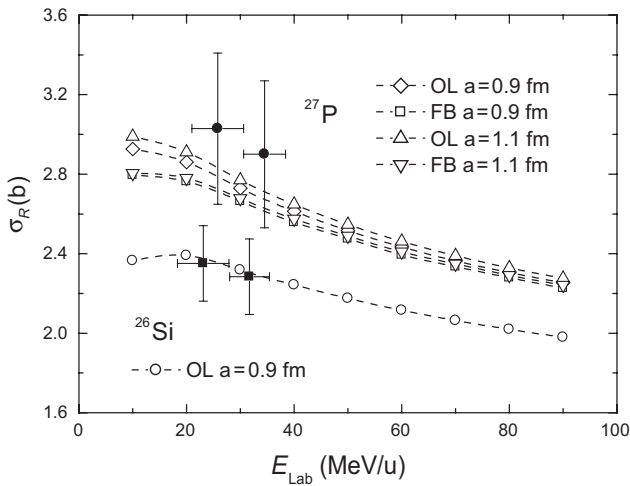


**Figure 3.** The measured reaction cross sections as a function of energy for the  $^{26}\text{Si}$ ,  $^{27}\text{P} + ^{28}\text{Si}$  reactions. The predictions of the modified Glauber model of OL and FB approaches (open symbols) are compared with the experimental data. The numbers in the figure represent the diffuseness parameter of the Woods-Saxon potential for the valence proton.

are one-proton halos in  $^{26,27,28}\text{P}$  and two-proton halos in  $^{27,28,29}\text{S}$ . In order to search proton halo, the reaction cross sections of  $^{27,28}\text{P}$ ,  $^{29}\text{S}$  and the corresponding isotones on Si target<sup>8,9</sup> were measured at intermediate energies. As shown in Figure 1, the measured reaction cross sections of the  $N=12$  and  $13$  isotones show an abrupt increase at  $Z=15$ . The experimental results for the isotones with  $Z \leq 14$  as well as  $^{28}\text{P}$  can be well described by the modified Glauber theory of the optical limit (OL) approach. The enhancement of the reaction cross sections for  $^{28}\text{P}$  could be explained in the modified Glauber theory with an enlarged core as illustrated in Figure 2. The  $\langle r_c^2 \rangle^{1/2}$  and  $\langle r_h^2 \rangle^{1/2}$  are the rms radii of the core and valence proton in  $^{28}\text{P}$ , respectively. The difference between the rms radii of the core and bare nuclei  $^{27}\text{Si}$  is about 0.15 fm. It is seen from Figure 3 that theoretical analysis with the modified Glauber theory of the OL and few-body (FB) approaches<sup>10-13</sup> underpredicts the experimental data of  $^{27}\text{P}$ . The difference between the rms radii of the core and bare nuclei  $^{26}\text{Si}$  is about 0.28 fm. Our theoretical analysis shows that an enlarged core together with proton halo are probably the mechanism responsible for the enhancement of the cross sections for the reaction of  $^{27}\text{P} + ^{28}\text{Si}$ . Ozawa et al.<sup>14</sup> proposed to take a difference factor as a possible measure of halo appearance. The difference factor  $d$  is defined as

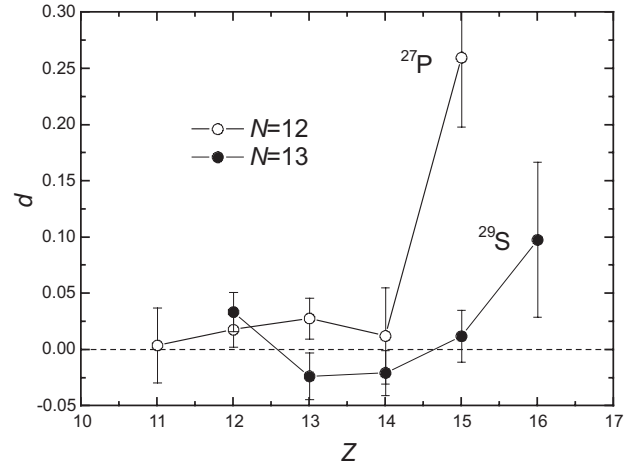


**Figure 4.**  $Z$  dependence of the different factor  $d$  for  $N=12$  and  $13$  isotones. The symbols are connected by lines to guide the eye.

$$d = \frac{\sigma_R(\text{exp}) - \sigma_R(\text{cal})}{\sigma_R(\text{cal})}, \quad (1)$$

here  $\sigma_R(\text{exp})$  represents the measured total reaction cross sections and  $\sigma_R(\text{cal})$  is the theoretical values with the modified Glauber theory of the OL and FB approaches. Figure 4 displays the  $Z$  dependence of  $d$  for  $N=12$  and  $13$  isotones at 40 MeV/u. We find from the  $d$  values that  $^{27}\text{P}$  and  $^{29}\text{S}$  have a proton halo and a moderate proton halo structure, respectively.

### 3. Nuclear Halo of Excited State

Except the nuclei near or at drip-lines, halo may appear in the excited states of stable nuclei. By means of the asymptotic normalization coefficients (ANC's) extracted from transfer reactions of  $^{11}\text{B}(d, p)^{12}\text{B}$ ,  $^{12}\text{C}(d, p)^{13}\text{C}$ , and  $\text{H}(^6\text{He}, n)^6\text{Li}$ , we have verified that the second ( $J^\pi = 2^-$ ) and third ( $J^\pi = 1^-$ ) excited states in  $^{12}\text{B}$  and the first ( $J^\pi = 1/2^+$ ) excited state in  $^{13}\text{C}$  are the neutron halo states,<sup>15</sup> while the second excited state ( $3.56 \text{ MeV}$ ,  $J^\pi = 0^+$ ) in  $^6\text{Li}$  is a proton-neutron halo state.<sup>16</sup>

**3.1. Root-Mean-Square Radius.** The rms radius of valence-nucleon(s) in the orbit ( $nlj$ ) can be separated into the contributions from the interior and the asymptotic regions,<sup>15,17</sup>

$$\langle r^2 \rangle^{1/2} = \left[ \int_0^{R_N} r^4 \phi_{nlj}^2(r) dr + (C_{ANlj}^B)^2 \int_{R_N}^{\infty} r^2 W_{-\eta, l+1/2}^2(2kr) dr \right]^{1/2}. \quad (2)$$

Here  $\phi_{nlj}(r)$  is the single-particle radial wave-function in the ( $nlj$ ) bound state,  $C_{ANlj}^B$  is the nuclear ANC, and  $W_{-\eta, l+1/2}(2kr)$  the Whittaker function. The first term in the equation is somehow parameter dependant. The second term is model parameter independent, and gives more than 90%<sup>11</sup> contribution to the value of rms radius. Thus the uncertainty introduced by the parameters used is small. Hence,  $\langle r^2 \rangle^{1/2}$  evaluated in this way is a nearly parameter independent quantity which can be served as an ideal experimental observable for the examination of nuclear halo. The rms radii for the valence particle extracted from ANC values are listed in Table 1 for the excited states in  $^{12}\text{B}$  and  $^{13}\text{C}$ . In the table,  $r_c$  and  $R_{\text{sq}} = \sqrt{\frac{5}{3}(r_c^2 + 4)}$  in the unit of fm are the radii of the core nucleus and the square-well potential, respectively.<sup>18</sup>

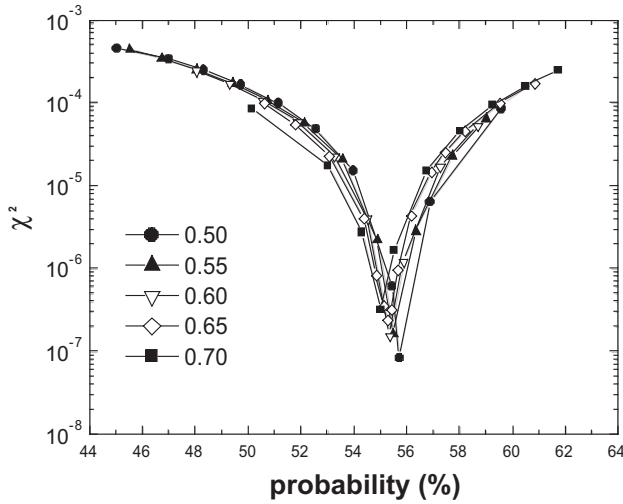
**3.2. Probability.** The probability<sup>15, 19</sup> for valence particle being out of the binding potential can be evaluated by,

$$P(R, r_0, a) = \frac{\int_R^{\infty} r^2 \phi_{nlj}^2(r) dr}{\int_0^{\infty} r^2 \phi_{nlj}^2(r) dr}, \quad (3)$$

where the  $r_0$  and  $a$  are the radius and diffuseness parameters of the potential, respectively. The binding potential radius  $R$  is

**TABLE 1: Values of  $\langle r^2 \rangle^{1/2}$  and  $\langle r^2 \rangle / r_c$ ,  $\langle r^2 \rangle / R_{sq}^2$  and the probability for valence nucleon being out of the binding potential for nucleus  $^{12}\text{B}$  and  $^{13}\text{C}$** 

Nucleus	$J^\pi$	$E_x$ (MeV)	$r_c$ (fm)	$\langle r^2 \rangle^{1/2}$ (fm)	$\langle r^2 \rangle^{1/2} / r_c$	$\langle r^2 \rangle / R_{sq}^2$	Probability (%)
$^{12}\text{B}$	$1^+$	0		$3.16 \pm 0.10$	$1.26 \pm 0.05$	$0.58 \pm 0.15$	19.9
	$2^-$	1.674	2.50	$4.01 \pm 0.61$	$1.60 \pm 0.29$	$1.10 \pm 0.31$	53.6
	$1^-$	2.621		$5.64 \pm 0.90$	$2.26 \pm 0.42$	$1.86 \pm 0.60$	66.8
$^{13}\text{C}$	$1/2^-$	0	2.42	$3.39 \pm 0.31$	$1.413 \pm 0.15$	$0.70 \pm 0.21$	14.3
	$1/2^+$	3.089		$5.04 \pm 0.75$	$2.08 \pm 0.37$	$1.55 \pm 0.47$	50.3

**Figure 5.** Dependence of the  $\chi^2$  on the probability ( $P$ ) for valence nucleon being out of the binding potential for the 2s excited state in  $^{13}\text{C}$ . Symbols are connected by a line for each  $a_0$  value to guide the eye.

taken as an equivalent square-well potential radius  $R_{sq}$ . Hence the single-particle wave functions are not determined uniquely. We search the potential parameters in such a way<sup>19</sup> that the quantity,

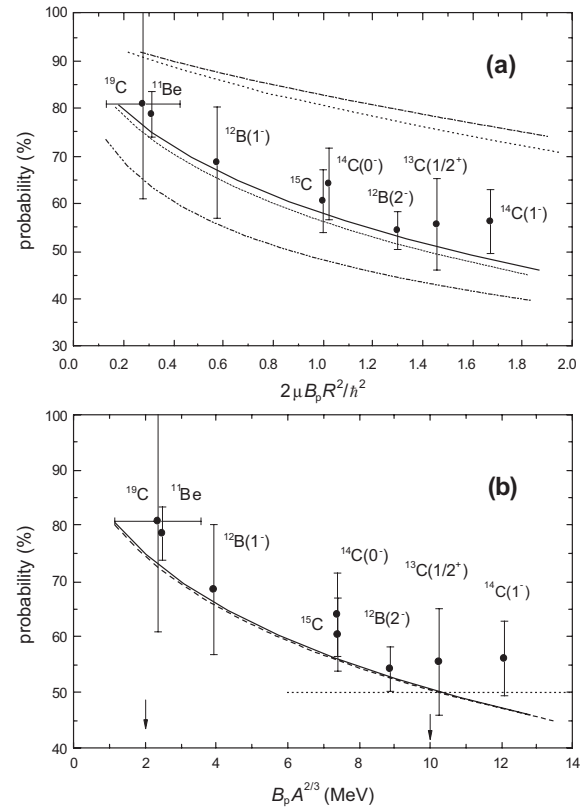
$$\chi_p^2 = \sum_{r_i=R_N}^{40\text{fm}} \left( [S_{ij}^{(sp)}]^{1/2} \phi_{nlj}(r_i) - C_{Aplj}^B \frac{W_{-\eta, l+1/2}(2kr_i)}{r_i} \right)^2, \quad (4)$$

becomes minimum. Where  $S_{ij}^{(sp)}$  is the single particle spectroscopic factor. First, the single-particle wave function is calculated with Woods-Saxon potential. The depth of the potential is adjusted to reproduce the binding energy. The values of  $a$  are chosen in the range of 0.50–0.70 fm. For each fixed  $a$ ,  $r_0$  is varied in a small step till the minimum in  $\chi_p^2$  is reached. In the calculation of  $\chi_p^2$ , the summation runs from  $r_i=6.0$  to 40 fm in steps of 0.1 fm. We find that the values of  $\chi_p^2$  does not change as long as  $R_N \geq 6$  fm. Figure 5 shows a typical example for the extraction of the probability for valence nucleon(s) being out of the binding potential. With this procedure, available data regarding the nuclear halo candidates are systematically analyzed and a number of halo nuclei are confirmed. The extracted probabilities for  $^{12}\text{B}$  and  $^{13}\text{C}$  are also listed in Table 1. Figure 6 shows the probability for valence nucleon being out of the binding potential as a function of  $2\mu B_p R^2 / \hbar^2$  (a) and  $B_p A^{2/3}$  (b). Based on these results and according to the probability of finding valence particle outside the bounding potential larger than 50%, we have got a condition for nuclear halo occurrence,<sup>19</sup>

$$B_p A^{2/3} \leq 10 \text{ MeV}. \quad (5)$$

Therefore, the range of nuclear halo occurrence is much expanded than the previous one,<sup>16</sup> i.e.,  $B_p A^{2/3} \leq 2$  MeV.<sup>20</sup> Here  $B_p$  is the binding energy of the valence nucleon and  $A$  is the mass number of the nucleus.

**3.3. Scaling Law.** Hamamoto et al.<sup>21</sup> have obtained the expressions of the expectation value for the operator  $r^2$  in a

**Figure 6.** Probability for valence nucleon being out of the binding potential as a function of  $2\mu B_p R^2 / \hbar^2$  (a) and  $B_p A^{2/3}$  (b). The solid points represent the s-wave halos in the ground state and in the excited states with spin and parity values in brackets, respectively. The dash-double-dotted line is the calculation value by means of the single-particle model with square-well potential. The other lines show the predictions of the single-particle models with Woods-Saxon potentials.<sup>19</sup> The arrows in the panel (b) illustrate the up-limits of  $B_p A^{2/3}$  value set by Jensen et al.<sup>20</sup> and by us.

finite square-well potential. The terms with  $\xi_0^4$  in denominator in their expressions are of negligible magnitude as compared to the other terms for the case of  $\chi^2 < 2$  which we are interested in. After omitting them, we get the following scaling laws for the dimensionless quantity  $\langle r^2 \rangle / R^2$ ,

$$\frac{\langle r^2 \rangle}{R^2} = \frac{1}{\chi+1} \left( 1 - \frac{\chi^2}{\xi_0^2} \right) \left( 1 + \frac{1}{\chi} + \frac{1}{2\chi^2} \right) + \chi \left( \frac{1}{3} + \frac{1+2\chi}{2\xi_0^2} \right) \quad \text{at } l=0, \quad (6)$$

$$\frac{\langle r^2 \rangle}{R^2} = \frac{1}{\chi^2+3\chi+3} \left[ \left( 1 - \frac{\chi^2}{\xi_0^2} \right) \left( \frac{(1+\chi)^2}{3} + \chi+3 + \frac{5}{2\chi} \right) + \frac{(1+\chi)^2}{2\xi_0^2} \right] + \frac{(2+2\chi+\chi^2)}{3\xi_0^2} \quad \text{at } l=1, \quad (7)$$

where

$$\chi = R \sqrt{\frac{2\mu B_p}{\hbar^2}}, \quad (8)$$

$$\xi_0 = R \sqrt{\frac{2\mu U_0}{\hbar^2}}. \quad (9)$$

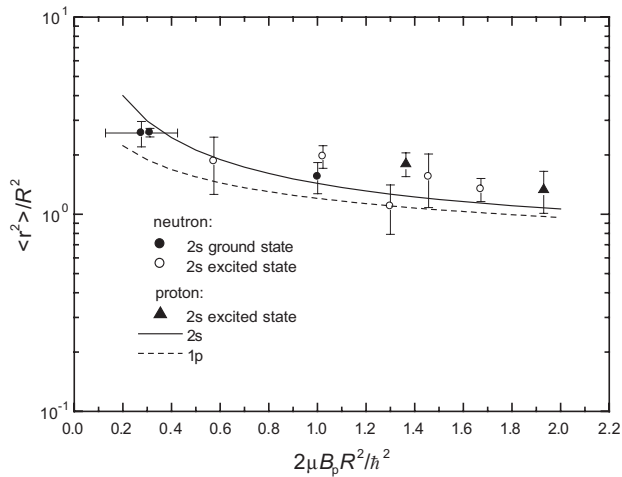


**Figure 7.** The experimental data of  $\langle r^2 \rangle / R^2$  vs  $2\mu B_p R^2 / \hbar^2$  for the valence nucleon in 2s state. The solid and dashed lines show the scaling laws of eqs 6 and 7.

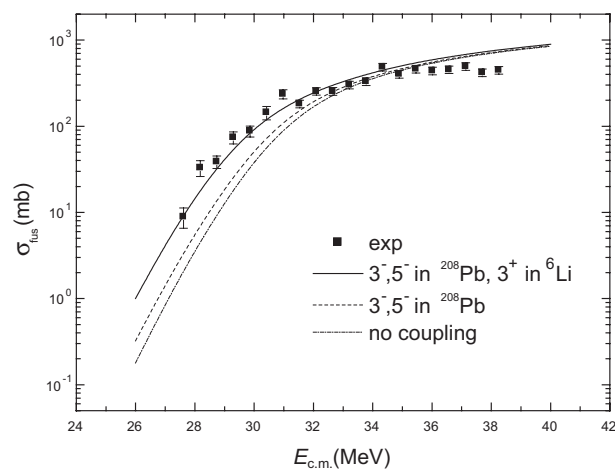


**Figure 8.** Total fusion cross sections for  ${}^6\text{Li} + {}^{208}\text{Pb}$ . The solid squares are the results of our experiment. The solid, dashed and dash-dotted lines are the results of the coupled-channels code CCFULL calculations with coupling the  $3^-$ ,  $5^-$  excitation states in  ${}^{208}\text{Pb}$  and the  $3^+$  excitation state in  ${}^6\text{Li}$  and with coupling the  $3^-$ ,  $5^-$  excitation states in  ${}^{208}\text{Pb}$ , as well as without coupling, respectively.

In the above equations,  $U_0$  is the depth and  $R$  is the range of the finite square-well potential and  $\mu$  and  $B_p$  the reduced mass and binding energy, respectively. Figure 7 displays the scaling laws for the dimensionless quantity  $\langle r^2 \rangle / R^2$  of the halo nuclei with comparison of experimental data. It can be seen from the figure that the scaling law can account for the available experimental data of halo candidates, even though it is derived in a finite square-well potential.

#### 4. Reactions Induced by Weakly Bound Nuclei

We have measured the complete fusion cross sections of  ${}^6\text{Li} + {}^{208}\text{Pb}$ , and found that the fusion cross sections above the Coulomb barrier are suppressed due to the breakup effects of weakly bound projectile  ${}^6\text{Li}$ .<sup>22</sup> The experimental results together with the theoretical calculations are shown in Figure 8. The lines in the figure are the coupled-channels code CCFULL calculations.<sup>23-25</sup> The deformation parameters used in the calculations (assuming single phonon excitations) are  $\beta_3 = 0.161$ <sup>25</sup>; and  $\beta_5 = 0.056$ <sup>27</sup> for  $3^-$  (2.615 MeV) and  $5^-$  (3.198 MeV) states in  ${}^{208}\text{Pb}$ , respectively, and  $\beta_2 = 1.51$ <sup>28</sup> for the  $3^+$  (2.186 MeV) in  ${}^6\text{Li}$ . The coupled-channels model (CCFULL) does not consider the influence of breakup effect on fusion.

We have also measured the elastic and quasi-elastic excitation functions of  ${}^6,7\text{Li}$ ,  ${}^9\text{Be} + {}^{208}\text{Pb}$  at backward angles. From these excitation functions, barrier distributions<sup>29</sup> are extracted

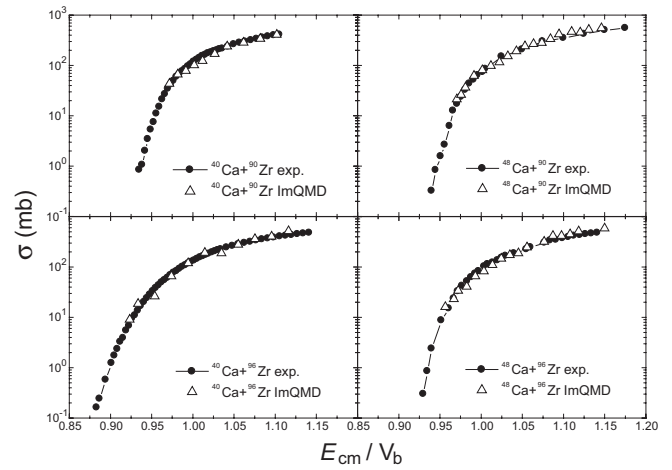


**Figure 9.** The fusion cross sections for  ${}^{40,48}\text{Ca} + {}^{90,96}\text{Zr}$ . The solid circles denote the experimental data. The open triangles denote the calculation results with the ImQMD model, respectively.

and compared with the predictions of the coupled-channels model. It is found that the barrier distributions are broadened and shifted to lower energies which may be a signature of the breakup effects of the weakly bound projectiles. Gomes et al.<sup>30</sup> study the behavior of the fusion, breakup reaction, and elastic scattering of different projectiles on  ${}^{64}\text{Zn}$  at near and above barrier energies. They found that the elastic (noncapture) breakup cross section is important at energies close to and above the Coulomb barrier and increases the reaction cross sections. In addition, they showed that the breakup process at near and below barrier energies is responsible for the vanishing of the usual threshold anomaly of the optical potential and gives rise to a new type of anomaly. Recently, Newton et al.<sup>31</sup> systematically analyzed the high precision fusion cross sections for  $Z_p Z_t < 1000$  with the coupled channels models and found that fits to the experimental fusion excitation functions need a value of  $a$  of the Woods-Saxon potential from 0.75 to 1.5 fm, which is much larger than the commonly accepted value of  $\approx 0.65$  fm. They think the large value of  $a$  may indicate the necessity to go beyond the potential model, and incorporate dynamical effects as the two nuclei move towards fusion, even for light systems with  $Z_p Z_t < 1000$ .

#### 5. Fusion Reactions with Neutron-Rich Nuclei

The dynamical effects on fusion of neutron-rich nuclei at the energies around the Coulomb barrier attract much attention in recent years. We have cooperated with Stefanini group from LNL/INFN to measure the fusion cross sections of  ${}^{48}\text{Ca} + {}^{90,96}\text{Zr}$  at the XTU-16 Tandem accelerator facility of the Laboratori Nazionali di Legnaro, Italy. Scarlassara et al.<sup>3</sup> have reported the preliminary experimental results of the reactions  ${}^{48}\text{Ca} + {}^{90,96}\text{Zr}$  in the International Conference FUSION03 at Matsushima, Miyagi, Japan. The comparison of experimental  ${}^{40,48}\text{Ca} + {}^{90,96}\text{Zr}$  fusion data<sup>2,3</sup> shows that fusion of  ${}^{40}\text{Ca} + {}^{96}\text{Zr}$  is much enhanced at near- and sub-barrier energies due to the positive Q-values of the transfer channels. The much larger enhancement for the  ${}^{40}\text{Ca} + {}^{96}\text{Zr}$  as compared to other three systems clearly indicates that neutron transfer with the positive Q-value should play a significant role in sub-barrier fusion. In order to extract the information on the complex dynamical effect, especially the effect of excess neutrons on fusion reactions, we have calculated the fusion excitation functions with the improved quantum molecular dynamics model<sup>4,32</sup> for the systems of  ${}^{40,48}\text{Ca} + {}^{90,96}\text{Zr}$  around the Coulomb barrier and compared with the experimental data of these four systems in Figure 9. It is shown by this comparison that neutron transfer starts far before the system reaches the top of the barrier and

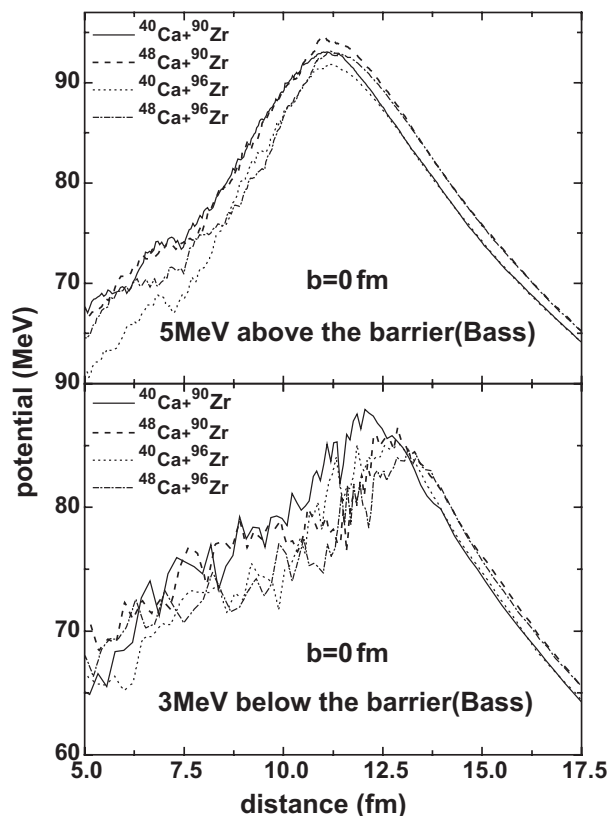


**Figure 10.** The dynamic barrier as a function of the distance between the centers of mass of projectile and target for head on reactions of  $^{40,48}\text{Ca} + ^{90,96}\text{Zr}$  at the incident energy of 5 MeV above and 3 MeV below the Bass barrier, respectively.

the flow of neutron between the reaction partners results in the neck formation. Consequently, the fusion barriers are strongly affected by the neutron transfer. Our calculations indicate that the neck grows faster and the distance between two partners is shorter for  $^{40}\text{Ca} + ^{96}\text{Zr}$  than other three systems, resulting a stronger reduction of the dynamic barrier as shown in Figure 10. We, therefore, can attribute from this calculation that the reduction of the barrier encountered by  $^{40}\text{Ca} + ^{96}\text{Zr}$  is due to the strong dynamical effect of the neutron transfer, which leads to the enhancement of the sub-barrier fusion cross sections for  $^{40}\text{Ca} + ^{96}\text{Zr}$ .

In very recent, Stefanini et al.<sup>33</sup> calculated the fusion excitation functions and barrier distributions for the  $^{48}\text{Ca} + ^{90,96}\text{Zr}$  systems by means of coupled-channels theory with CCFULL code. The sub-barrier fusion of  $^{48}\text{Ca} + ^{90}\text{Zr}$  is reproduced by coupled-channels calculations including the lowest quadrupole and octupole vibrations of  $^{90}\text{Zr}$ , and using a Woods-Saxon potential with standard diffuseness parameter  $a=0.68$  fm. However, the fusion cross sections are overestimated above the barrier. The low-energy slope of the excitation function for  $^{48}\text{Ca} + ^{96}\text{Zr}$  is steeper. This implies a larger diffuseness parameter  $a=0.85$  fm. Fusion cross sections are well fit in the whole energy region, and the effect of the strong octupole vibration in  $^{96}\text{Zr}$  is predominant. The extracted fusion barrier distributions are reasonably well reproduced by calculations for both systems. A comparison with previous data for  $^{40}\text{Ca} + ^{90,96}\text{Zr}$  is made in an attempt to clarify the role of transfer couplings in sub-barrier fusion.

## 5. Summary

The reaction cross sections of  $^{27,28}\text{P}$ ,  $^{29}\text{S}$  and the corresponding isotones on Si target were measured at intermediate energies. The theoretical analysis with the modified Glauber theory of the optical limit and few-body approaches underpre-

dicts the experimental data of  $^{27}\text{P}$ . Our theoretical analysis shows that an enlarged core together with proton halo are probably the mechanism responsible for the enhancement of the cross sections for the reaction of  $^{27}\text{P} + ^{28}\text{Si}$ . We find from the different factor values that  $^{29}\text{S}$  may have a moderate proton halo structure. By means of the asymptotic normalization coefficients extracted from transfer reactions of  $^{11}\text{B}(d, p)^{12}\text{B}$  and  $^{12}\text{C}(d, p)^{13}\text{C}$ , we have verified that the second ( $J^\pi=2^-$ ) and third ( $J^\pi=1^-$ ) excited states in  $^{12}\text{B}$  and the first ( $J^\pi=1/2^+$ ) excited state in  $^{13}\text{C}$  are the neutron halo states. The probability of the valence nucleon(s) being out of the binding potential have been extracted systematically from the relevant experimental data and a much relaxed condition for nuclear halo occurrence proposed. Based on our systematical study, we put forward our scaling laws of nuclear halo in terms of the analytical expressions of the expectation value for the operator  $r^2$  in a finite square-well potential. In order to investigate the breakup effects of the weakly bound projectiles on fusion reactions and barrier distributions, the complete fusion cross sections of  $^6\text{Li} + ^{208}\text{Pb}$  and the elastic and quasi-elastic excitation functions of  $^{6,7}\text{Li}, ^9\text{Be} + ^{208}\text{Pb}$  were measured at the back angles and compared with the predictions of the coupled-channels model. It is found that the fusion cross sections above the Coulomb barrier are suppressed due to the breakup effects of weakly bound projectile  $^6\text{Li}$  and the barrier distributions are somehow broaden and shift to lower energies. The dynamical effects on fusion of neutron-rich nuclei at the energies around the Coulomb barrier are discussed in terms of the comparison of the measured fusion data of  $^{48}\text{Ca} + ^{90,96}\text{Zr}$  with the calculations of the ImQMD model. Our study shows that the dynamical effects triggered by the neutron transfer play important role in fusion reactions. We also introduce the very recent results calculated with coupled-channels theory.

**Acknowledgments.** This work was supported by the National Natural Science Foundation of China under Grant No. 10275092, 10275095, 10235030.

## References

- (1) I. Tanihata, H. Hamagaki, O. Hashimoto, Y. Shida, and N. Yoshikawa, Phys. Rev. Lett. **55**, 2676 (1985).
- (2) H. Timmers, D. Ackermann, S. Beghini, L. Corradi, J. H. He, G. Montagnoli, F. Scarlassara, A. M. Stefanini, and N. Rowley, Nucl. Phys. A**633**, 421 (1998).
- (3) F. Scarlassara, G. Montagnoli, S. Beghini, R. Silvestri, A. M. Stefanini, L. Corradi, B. R. Behera, E. Fioretto, S. Szilner, M. Trotta, Y. W. Wu, Z. H. Liu, M. Ruan, F. Yang, and H. Q. Zhang, Prog. Theor. Phys. Suppl. **154**, 31 (2004).
- (4) N. Wang, Z. Li, and X. Wu, Phys. Rev. C **69**, 034608 (2004).
- (5) Z. Ren, B. Chen, Z. Ma, and G. Xu, Phys. Rev. C **53**, R572 (1996).
- (6) B. A. Brown and P. G. Hanson, Phys. Lett. B **381**, 391 (1996).
- (7) B. Q. Chen, Z. Y. Ma, F. Grummer, and S. Krewald, J. Phys. G: Nucl. Part. Phys. **24**, 97 (1998).
- (8) Z. H. Liu, M. Ruan, Y. L. Zhao, H. Q. Zhang, F. Yang, Z. Y. Ma, C. J. Lin, B. Q. Chen, Y. W. Wu, W. L. Zhan, Z. Y. Guo, G. Q. Xiao, H. S. Xu, Z. Y. Sun, J. X. Li, and Z. J. Chen, Phys. Rev. C **69**, 034326 (2004).
- (9) Z. H. Liu, M. Ruan, Y. L. Zhao, H. Q. Zhang, F. Yang, Z. Y. Ma, C. J. Lin, B. Q. Chen, Y. W. Wu, W. L. Zhan, Z. Y. Guo, G. Q. Xiao, H. S. Xu, Z. Y. Sun, J. X. Li, and Z. J. Chen, Chin. Phys. Lett. **21**, 1711 (2004).
- (10) Y. Ogawa, K. Yabana, and Y. Suzuki, Nucl. Phys. A**543**, 723(1992).
- (11) J. S. Al-khalili and J. A. Tostevin, Phys. Rev. Lett. **76**, 3903(1996).

- (12) Y. L. Zhao, Z. Y. Ma, and B. Q. Chen, *Commun. Theor. Phys.* **36**, 313(2001).
- (13) Y. L. Zhao, Z. Y. Ma, B. Q. Chen, and W. Q. Shen, *Chin. Phys. Lett.* **20**, 53(2003).
- (14) A. Ozawa, I. Tanihata, T. Kobayashi, Y. Sugahara, O. Yamakawa, K. Omata, K. Sugimoto, D. Olson, W. Christie, and H. Wieman, *Nucl. Phys. A* **608**, 63 (1996).
- (15) Z. H. Liu, C. J. Lin, H. Q. Zhang, Z. C. Li, J. S. Zhang, Y. W. Wu, F. Yang, M. Ruan, J. C. Liu, S. Y. Li, and Z. H. Peng, *Phys. Rev. C* **64**, 034312 (2001).
- (16) Z. H. Li, W. P. Liu, X. X. Bai, Y. B. Wang, G. Lian, Z. C. Li, and S. Zeng, *Phys. Lett.* **B527**, 50 (2002).
- (17) A. M. Mukhamedzhanov, C. A. Gagliardi, and R. E. Tribble, *Phys. Rev. C* **63**, 024612 (2001).
- (18) D. V. Fedorov, A. S. Jensen, and K. Riisager, *Phys. Lett.* **B312**, 1 (1993).
- (19) Z. H. Liu, X. Z. Zhang, and H. Q. Zhang, *Phys. Rev. C* **68**, 024305 (2003).
- (20) A. S. Jensen and K. Riisager, *Phys. Lett.* **B480**, 39 (2000).
- (21) I. Hamamoto and X. Z. Zhang, *Phys. Rev. C* **58**, 3388 (1998).
- (22) Y. W. Wu, Z. H. Liu, C. J. Lin, H. Q. Zhang, M. Ruan, F. Yang, Z. C. Li, M. Trotta, and K. Hagino, *Phys. Rev. C* **68**, 044605 (2003).
- (23) K. Hagino, N. Takigawa, M. Dasgupta, D. J. Hind, and J. R. Leigh, *Phys. Rev. C* **55**, 276 (1997).
- (24) K. Hagino, N. Takigawa, M. Dasgupta, D. J. Hind, and J. R. Leigh, *Phys. Rev. Lett.* **79**, 2014 (1997).
- (25) K. Hagino, N. Takigawa, and S. Kuyucak, *Phys. Lett.* **79**, 2943 (1997).
- (26) R. H. Spear, *At. Data Nucl. Data Tables* **42**, 55 (1989).
- (27) D. K. McDaniels, J. Lisantti, I. Bergqvist, L. W. Swenson, X. Y. Chen, D. J. Horen, F. E. Bertrand, E. E. Gross, C. Glover, R. Sayer, B. L. Burks, O. Hausser, and K. Hicks, *Nucl. Phys. A* **467**, 557 (1987).
- (28) F. Ajzenberg-Selove, *Nucl. Phys. A* **413**, 1 (1984).
- (29) H. Timmer, J. R. Leigh, M. Dasgupta, D. J. Hinde, R. C. Lemmon, J. C. Mein, C. R. Morton, J. O. Newton, and N. Rowley, *Nucl. Phys. A* **594**, 190 (1995).
- (30) P. R. S. Gomes, M. D. Rodriguez, G. V. Marti, I. Padron, L. C. Chamon, J. O. Fernandez Niello, O. A. Capurro, A. J. Pachco, J. E. Testoni, A. Arazi, M. Ramirez, R. M. Anjos, J. Lubian, R. Veiga, R. Liguori Neto, E. Crema, N. Added, C. Tenreiro, and M. S. Hussein, *Phys. Rev. C* **71**, 034608 (2005).
- (31) J. O. Newton, R. D. Butt, M. Dasgupta, D. J. Hinde, I. I. Gontchar, and C. R. Morton, *Phys. Rev. C* **70**, 024605 (2004).
- (32) Z. Kai, L. Zhuxia, W. Ning, Z. Yingxun, and T. Junlong, *High Energy Physics and Nuclear Physics* **30**, 26 (2006).
- (33) A. M. Stefanini, F. Scarlassara, S. Beghini, G. Montagnoli, R. Silvestri, M. Trotta, B. R. Behera, L. Corradi, E. Fioretto, A. Gadea, Y. W. Wu, S. Szilner, H. Q. Zhang, Z. H. Liu, M. Ruan, F. Yang, and N. Rowley, *Phys. Rev. C* **73**, 034606 (2006).